Journal of Mining and Environment (JME) Vol. 17, No. 5, 2026, 1691-1713

Shahrood University of Technology

Journal of Mining and Environment (JME)

Journal homepage: www.jme.shahroodut.ac.ir

Iranian Society of Mining Engineering (IRSME)

An Integrated FDM–GA Framework for Automated Back Analysis in Tunneling–Part II: Case Study and the Influence of Stress Relaxation Parameters

Mohammad-Taghi Hamzaban[1*], Alireza Chehreghan[2], and Roozbeh Geraili Mikola[3]

1. Associate Professor, Mining Engineering Faculty, Sahand University of Technology, Tabriz, Iran.
2. Associate Professor, Mining Engineering Faculty, Sahand University of Technology, Tabriz, Iran.
3. Lead Associate, Delve Underground, Walnut Creek, CA, USA

Article Info

Received 6 December 2025
Received in Revised form 25 July 2026
Accepted 31 July 2026
Published online 31 July 2026

DOI: 10.22044/jme.2026.17275.3422

Keywords

Tunnel
Numerical Modeling
Back Analysis
Genetic Algorithm
Stress relaxation

Abstract

In the companion Part I paper, an integrated Finite Difference Method–Genetic Algorithm (FDM–GA) framework was developed for automated tunnel back analysis, coupling numerical simulation with evolutionary optimization to estimate geotechnical parameters from field monitoring data. Part II demonstrates the application and validation of this framework through the back analysis of the Pardis Highway Tunnel, excavated within the Hezar Darreh conglomerate formation in northern Tehran, Iran. Three-point convergence measurements from 24 monitoring stations were processed to derive representative reference displacements for calibration. Thirty independent FDM–GA optimization runs were performed to estimate the ground parameters, yielding narrow calibrated ranges for cohesion (c), friction angle (φ), Young's modulus (E), and the coefficient of lateral earth pressure at rest (K0). A representative engineering parameter set was identified by integrating optimization results with inter-parameter correlations and geotechnical evidence from comparable tunnel projects. Unlike conventional tunnel back analysis studies that primarily emphasize parameter optimization, the proposed framework integrates optimization with geological interpretation to identify representative engineering parameter sets. It also systematically evaluates how stress relaxation assumptions influence parameter calibration and the engineering interpretation of calibrated solutions. Recalculated Ground Reaction Curve (GRC) and Longitudinal Displacement Profile (LDP) showed that relatively small variations in stress relaxation assumptions significantly affect predicted convergence and calibrated geotechnical parameters. The results demonstrate that reliable estimation of pre-support deformation and stress release is essential for realistic tunnel back analysis and confirm that the integrated FDM–GA framework provides a robust, repeatable tool for geotechnical parameter calibration in NATM tunnel engineering.

1. Introduction

Back analysis is a fundamental tool in tunnel engineering for identifying geotechnical parameters that cannot be measured directly or estimated with sufficient accuracy through field or laboratory testing. By minimizing the discrepancy between observed field responses and numerical model predictions, back analysis provides a rational basis for calibrating constitutive parameters and refining numerical models. In the companion Part I paper, an integrated back analysis framework coupling the Finite Difference Method (FDM) and a simplified Genetic Algorithm (GA) was developed and verified within the FISH programming environment of the FLAC^{2D} software. The proposed framework demonstrated its effectiveness in synthetic tunnel problems by capturing the inherent non-uniqueness of inverse analysis while revealing meaningful inter-parameter correlations.

Corresponding author: hamzaban@sut.ac.ir (M.T. Hamzaban)

In recent years, tunnel back analysis has increasingly benefited from advances in optimization algorithms, machine-learning techniques, and surrogate modelling approaches. Population-based optimization methods, including genetic algorithms, particle swarm optimization, differential evolution, and other evolutionary techniques, have been widely employed to estimate geotechnical parameters by minimizing discrepancies between measured and numerically predicted tunnel responses [1-3]. More recently, machine-learning-assisted inverse analysis frameworks have been developed to improve computational efficiency through surrogate models based on artificial neural networks, Gaussian process regression, and other data-driven techniques [3-5]. These developments have broadened the applicability of inverse analysis methods to increasingly complex tunnelling problems.

Despite these methodological advances, several challenges remain. Many existing studies primarily emphasize optimization performance while giving limited attention to the non-uniqueness of calibrated solutions, the engineering interpretation of optimized parameter sets, and the influence of modelling assumptions on the final calibration results. In particular, the effects of stress relaxation assumptions, including both the stress relaxation factor and the stress relaxation rate adopted in two-dimensional (2D) tunnel analyses, have received comparatively little systematic investigation. Addressing these challenges requires methodologies that combine automated optimization with engineering judgement and geological interpretation to obtain representative and practically applicable parameter sets.

The present study extends the integrated FDM–GA framework developed in Part I through its application to the Pardis Highway Tunnel, excavated within the Hezar Darreh conglomerate formation in northern Tehran, Iran. The geological complexity of the site, together with limited and spatially variable monitoring data, provides a suitable case study for validating the proposed framework under real engineering conditions. Three-point convergence measurements obtained from 24 monitoring stations were processed to provide the calibration dataset. Particular emphasis is placed on investigating the influence of the stress relaxation factor and stress relaxation rate on back analysis results. Although these parameters are routinely adopted in 2D numerical analyses to simulate face-induced deformation, their effects on calibrated geotechnical parameters have not been systematically quantified. Even relatively small variations in these assumptions may significantly influence predicted tunnel displacements, Ground Reaction Curve (GRC) and Longitudinal Displacement Profile (LDP) characteristics, and consequently the estimated geotechnical parameters. The objectives of Part II are therefore threefold:

- To apply the integrated FDM–GA framework to calibrate the governing geotechnical parameters of the Pardis Highway Tunnel using processed convergence measurements.
- To identify a representative and geologically consistent parameter set from multiple optimized solutions by integrating optimization results with independent geotechnical evidence and inter-parameter correlations.
- To systematically investigate how variations in the stress relaxation factor and rate affect back analysis results.

Unlike previous optimization-based tunnel back analysis studies, the present work combines automated parameter optimization with geological interpretation and systematic evaluation of stress relaxation assumptions. The framework is validated using comprehensive field measurements from 24 monitoring stations, and its repeatability is demonstrated through 30 independent optimization runs. These contributions provide a systematic and practical methodology for reliable geotechnical parameter calibration in NATM tunnels. Back analysis is a fundamental tool in tunnel engineering for identifying geotechnical parameters that cannot be measured directly or estimated with sufficient accuracy through field or laboratory testing. By minimizing the discrepancy between observed field responses and numerical model predictions, back analysis provides a rational basis for calibrating constitutive parameters and refining numerical models. In the companion Part I paper, an integrated back analysis framework coupling the Finite Difference Method (FDM) and a simplified Genetic Algorithm (GA) was developed and verified within the FISH programming environment of the FLAC^{2D} software. The proposed framework demonstrated its effectiveness in synthetic tunnel problems by capturing the inherent non-uniqueness of inverse analysis while revealing meaningful inter-parameter correlations.

In recent years, tunnel back analysis has increasingly benefited from advances in optimization algorithms, machine-learning techniques, and surrogate modelling approaches.

Population-based optimization methods, including genetic algorithms, particle swarm optimization, differential evolution, and other evolutionary techniques, have been widely employed to estimate geotechnical parameters by minimizing discrepancies between measured and numerically predicted tunnel responses [1-3]. More recently, machine-learning-assisted inverse analysis frameworks have been developed to improve computational efficiency through surrogate models based on artificial neural networks, Gaussian process regression, and other data-driven techniques [3-5]. These developments have broadened the applicability of inverse analysis methods to increasingly complex tunnelling problems.

Despite these methodological advances, several challenges remain. Many existing studies primarily emphasize optimization performance while giving limited attention to the non-uniqueness of calibrated solutions, the engineering interpretation of optimized parameter sets, and the influence of modelling assumptions on the final calibration results. In particular, the effects of stress relaxation assumptions, including both the stress relaxation factor and the stress relaxation rate adopted in two-dimensional (2D) tunnel analyses, have received comparatively little systematic investigation. Addressing these challenges requires methodologies that combine automated optimization with engineering judgement and geological interpretation to obtain representative and practically applicable parameter sets.

The present study extends the integrated FDM–GA framework developed in Part I through its application to the Pardis Highway Tunnel, excavated within the Hezar Darreh conglomerate formation in northern Tehran, Iran. The geological complexity of the site, together with limited and spatially variable monitoring data, provides a suitable case study for validating the proposed framework under real engineering conditions. Three-point convergence measurements obtained from 24 monitoring stations were processed to provide the calibration dataset. Particular emphasis is placed on investigating the influence of the stress relaxation factor and stress relaxation rate on back analysis results. Although these parameters are routinely adopted in 2D numerical analyses to simulate face-induced deformation, their effects on calibrated geotechnical parameters have not been systematically quantified. Even relatively small variations in these assumptions may significantly influence predicted tunnel displacements, Ground Reaction Curve (GRC) and Longitudinal Displacement Profile (LDP) characteristics, and consequently the estimated geotechnical parameters. The objectives of Part II are therefore threefold:

Unlike previous optimization-based tunnel back analysis studies, the present work combines automated parameter optimization with geological interpretation and systematic evaluation of stress relaxation assumptions. The framework is validated using comprehensive field measurements from 24 monitoring stations, and its repeatability is demonstrated through 30 independent optimization runs. These contributions provide

2. Pardis Highway Tunnel Project

To evaluate the performance of the proposed FDM–GA approach in a real-world setting, monitoring data from Tunnel No. 1 of the Pardis Highway Project, located in northern Tehran, Iran, were analyzed [6]. The tunnel, which features a horseshoe-shaped cross section, was excavated using a roadheader. The geological profile along the tunnel alignment is shown in Figure 1a, indicating that the tunnel primarily passes through the Hezar Darreh Formation. Figure 1b shows the corresponding excavated section of the tunnel during the top-heading excavation stage.

The available monitoring data were collected during the excavation of the top-heading section. The instrumentation system consisted of a set of three-point convergence pins used to measure the relative displacements of the tunnel walls and roof. A photograph of a convergence pin installed on the tunnel wall is shown in Figure 2a. The pins were arranged in a three-point configuration, as illustrated schematically in Figure 2b. The convergencemeter used to measure the relative displacement between pairs of opposing pins is shown in Figures 2c and 2d.

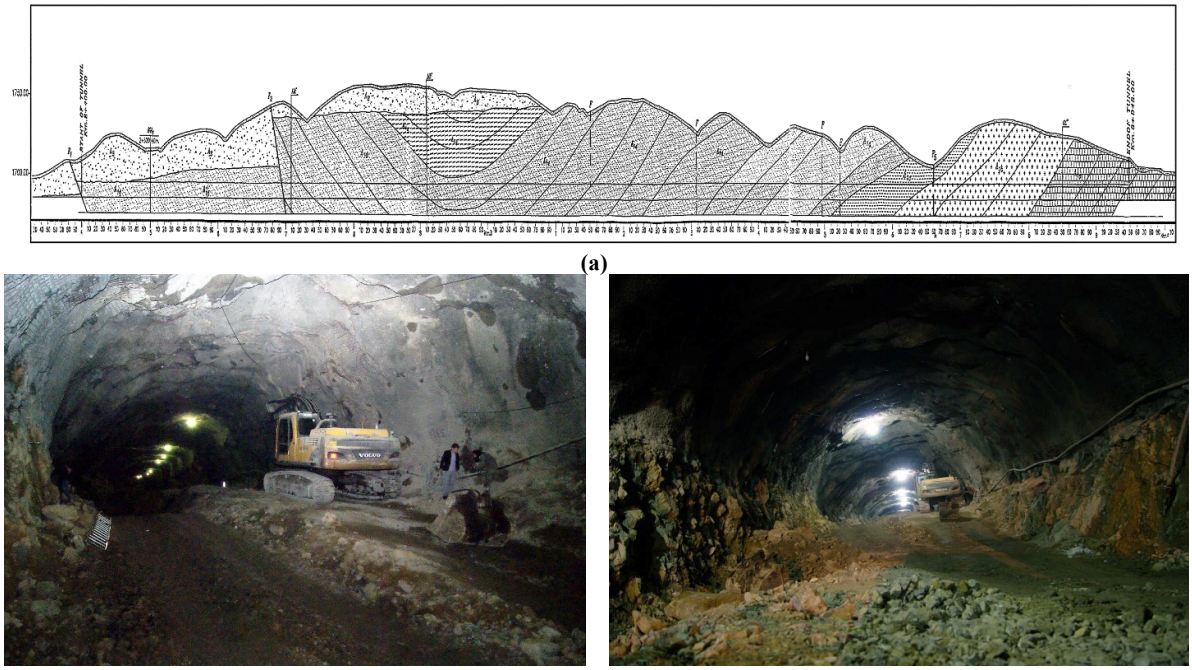

(a)

(b) (c)

Figure 1. (a) Geological profile along the alignment of Tunnel No. 1 in the Pardis Highway project, showing the predominance of the Hezar Darreh conglomerate formation and (b) Excavated tunnel section during the top-heading stage

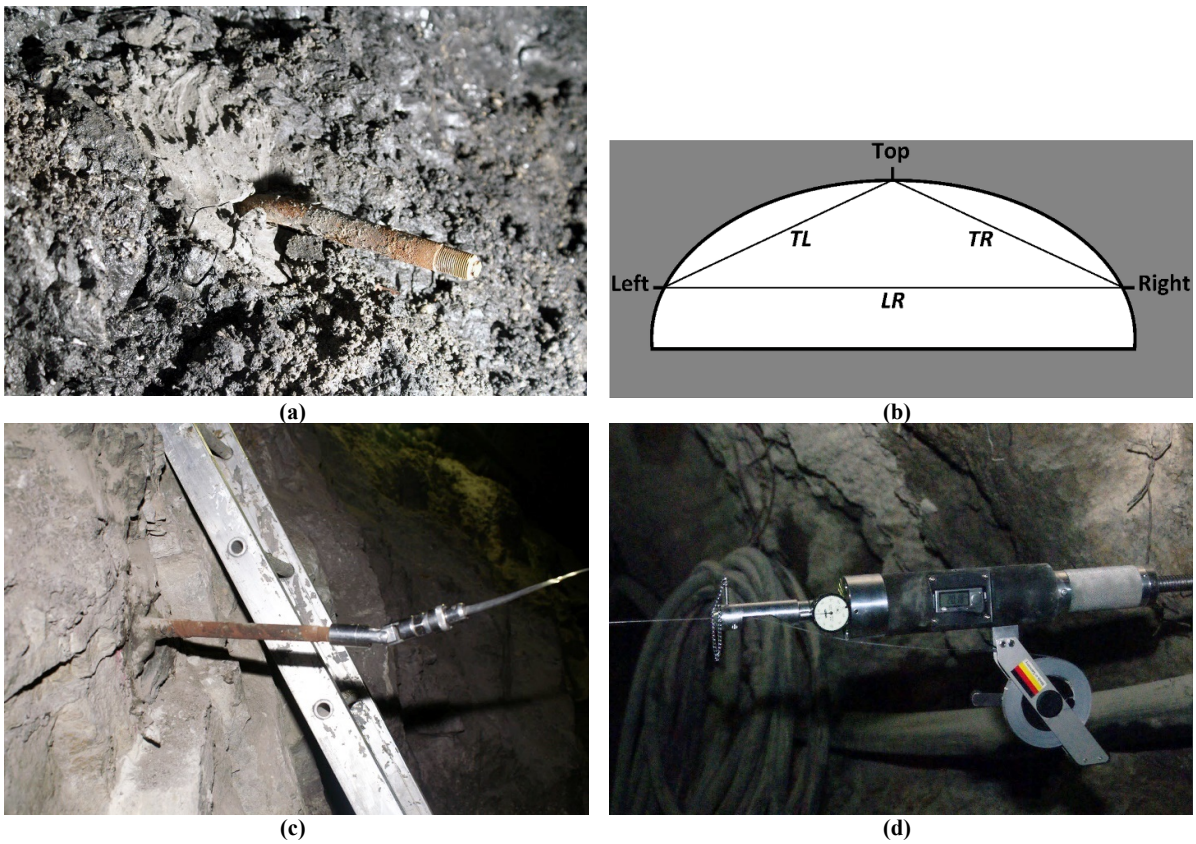

(a) (b)

(c) (d)

Figure 2. (a) Convergence pin installed on the tunnel wall, (b) Schematic illustration of the three-point pin arrangement, and (c, d) Convergencemeter setup used to measure relative displacements between opposite pins

The monitoring data from 24 convergence stations installed along the tunnel were analyzed to establish the calibration dataset for the back analysis process [7]. These stations were installed at varying distances from the tunnel face. The final measured convergence values were plotted against the tunnel face distances at the time of installation, which represent the distances between the tunnel face and the monitoring stations when the first convergence measurements were recorded (Figure 3). The resulting plots show power-law relationships between the final recorded convergence values and the installation distances for the Top-Left (TL), Top-Right (TR), and Left-Right (LR) measurements. As expected, stations located farther from the tunnel face recorded smaller convergence values because a substantial portion of the ground deformation had already occurred before the monitoring pins were installed. The fitted power-law relationships were then used to estimate the convergence values corresponding to a hypothetical installation distance of 2 m from the tunnel face. These estimated values were deemed representative convergence values and were used as calibration targets in the FDM–GA back analysis procedure. The representative convergence values for the TL, TR, and LR directions are summarized in Table 1.

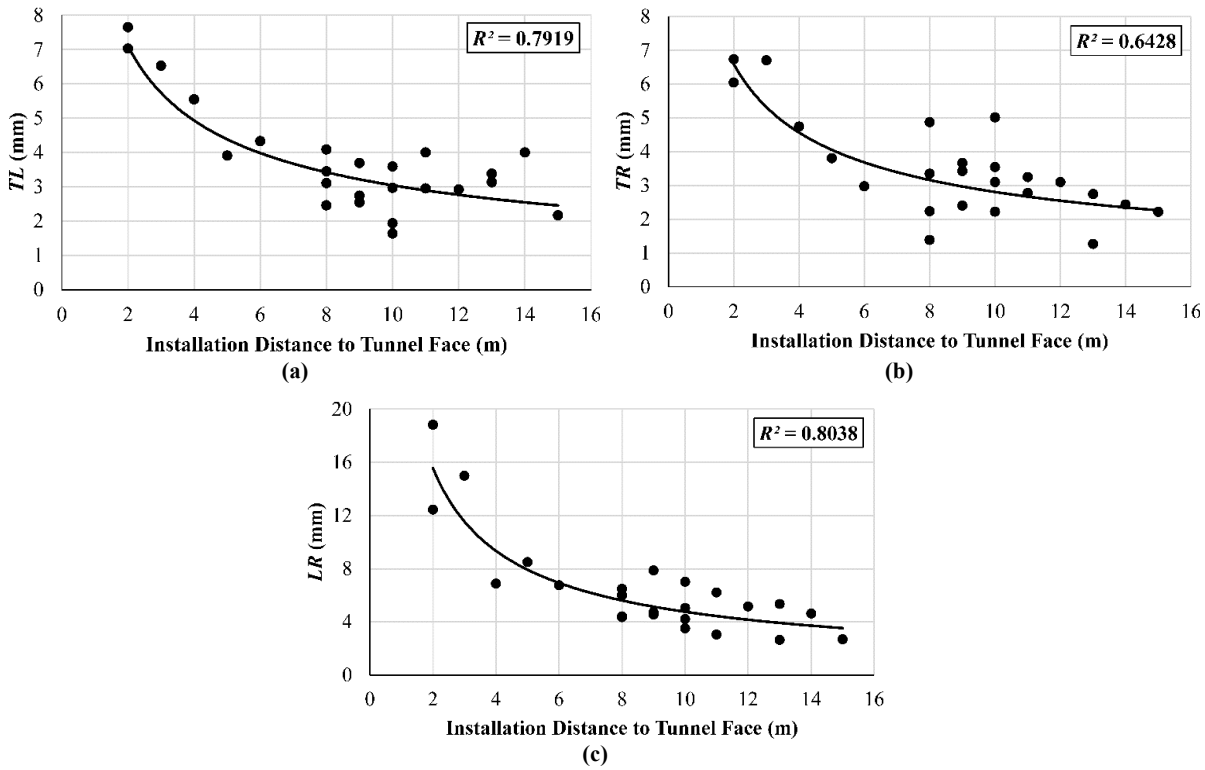

Figure 3. Relationship between final recorded convergence values and installation distance from the tunnel face for the (a) Top-Left (TL_m), (b) Top-Right (TR_m), and (c) Left-Right (LR_m) measurements

Table 1. Final Pardis tunnel monitoring data for example application [7]

TL_m (cm)	TR_m (cm)	LR_m (cm)
7.247	6.571	15.446

TL_m: Measured convergence along the Top-Left direction
TR_m: Measured convergence along the Top-Right direction
LR_m: Measured convergence along the Left-Right direction

The tunnel support system comprised 3-bar lattice girder steel sets and a 10 cm-thick shotcrete layer, which was installed 2 m behind the tunnel face [6].

Consistent with the verification examples presented in Part I, the geotechnical parameters calibrated through the back analysis procedure were mass density (ρ), Young's modulus (E), Poisson's ratio (υ), cohesion (c), friction angle (φ), and the coefficient of lateral earth pressure at rest (K_0).

3. Example Application of FDM–GA Back Analysis Framework

Conglomerate is a type of sedimentary rock composed of large rock fragments (≥ 2 mm) embedded in a finer-grained matrix [8]. Conglomerates exhibit considerable variability in their engineering properties due to differences in

the origin, shape, size, and composition of the rock fragments, as well as the characteristics of the matrix. Because the textural and mechanical properties of rocks are closely related [9-11], conglomerates exhibit substantial heterogeneity and a broad range of mechanical properties [12-17]. Table 2 summarizes the reported mechanical properties of conglomerate formations from various tunnelling and engineering projects in Iran, highlighting the significant variability among the investigated sites. No published data were found for the coefficient of lateral earth pressure at rest (K_0) for these formations. According to in-situ stress measurements reported by Hoek [18], K_0 may range from 0.5 to 3.0. However, considering the prevailing reverse faulting regime in the project area, the expected value of K_0 is likely to exceed 1.0 [19]. Based on the information summarized in Table 2 and the above considerations regarding K_0, the adopted ranges of the geotechnical parameters are presented in Table 3 and used as the search space for the subsequent back analysis procedure.

The selected genetic algorithm parameters were a population size (m) of 40, a survival rate (SR) of 0.4, and a mutation rate (MR) of 0.4. Since the unknown variables in the back analysis problem are identical to those considered in the verification examples presented in Part I, m, SR, MR values were kept unchanged. However, because the supported horseshoe-shaped tunnel section represents a more complex mechanical system than the unsupported circular tunnel used in the verification examples, the maximum number of consecutive iterations without improvement, used as the stopping criterion, was increased to 400.

Table 2. Reported geotechnical properties for conglomerate rock material in some projects in Iran

No.	ρ (kg/m^3)	E (GPa)	υ	c (kPa)	φ (°)	Reference
1	-	0.025 – 0.15	-	21	37	Tehran metro tunnels [20]
2	-	5.6	-	200	25	Tunnel no. 1 (Pardis Highway) [6]
3	-	3	-	500	35	Lavarak cavern [21]
4	-	0.05 – 0.1	-	20 – 45	30 – 34	Resalat tunnel [22, 23]
5	2100	2	0.27	170	33	Lavasan water tunnel [24]
6	2550 – 2650	0.7 – 3	0.24 – 0.37	280 – 760	45 – 54	QLT6 tunnel [12]

Table 3. Selected potential range of the ground geotechnical parameters based on the cases in Table 2 and the results of back analysis

	Selected range	Initial values for calculating LDP and GRC	Back analyzed range	Back analysis outcome
mass density – ρ (kg/m^3)	2100 – 2700	2400	2147 – 2684	2300
Young's modulus – E (GPa)	0.01 – 6.00	3.0	0.4374 – 1.1280	0.44
Poisson's ratio – υ	0.25 – 0.40	0.32	0.2535 – 0.3970	0.40
cohesion – c (kPa)	0 – 500	250	8.42 – 95.65	21
friction angle – φ (°)	20 – 40	30	20.22 – 36.76	33
K_0 coefficient	1 – 3	2	1.508 – 2.966	1.69

To initiate the analysis and perform the necessary calculations, the mean values of the selected geotechnical parameters listed in Table 3 were used to generate LDP and GRC curves using both three-dimensional (3D) and 2D numerical models, as shown in Figure 4. Since both the tunnel support system and the instrumentation were installed approximately 2 m behind the tunnel face, the LDP and GRC curves indicate that the tunnel crown undergoes a displacement of approximately 3.67 mm prior to the installation of the support system and convergence monitoring pins. This corresponds to a stress relaxation factor of approximately 83.5%. Accordingly, this initial displacement was incorporated into the 2D numerical model before the calculated convergence values were evaluated. However, the LDP and GRC curves were generated using preliminary estimates of the geotechnical parameters, which are themselves the unknown variables to be calibrated through the back analysis procedure. Consequently, the estimated initial displacement and corresponding stress relaxation factor may differ from their actual values. Such differences may influence the predicted displacements and, ultimately, the calibrated geotechnical parameters. Therefore, the initial estimates derived from Figure 4 were adopted only to establish the starting conditions for the optimization procedure. The influence of the calibrated parameter values on the LDP, GRC, stress relaxation factor, and back analysis results is investigated in the following sections.

Since the left and right pin installation locations and the measured convergence values are not symmetrical, the entire tunnel cross section was

modelled. Figure 5 shows the numerical grid and the excavated tunnel. The grid was designed to be finer around the tunnel, and three grid points were positioned at the exact locations of the convergence pins installed on the tunnel roof and walls to ensure the accurate calculation of displacements and minimize numerical interpolation errors.

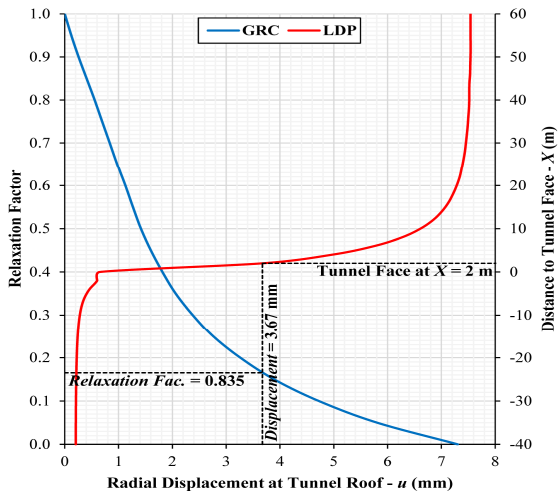

Figure 4. LDP and GRC curves for calculating the displacement and stress relaxation values before the installation of the instrumentation system

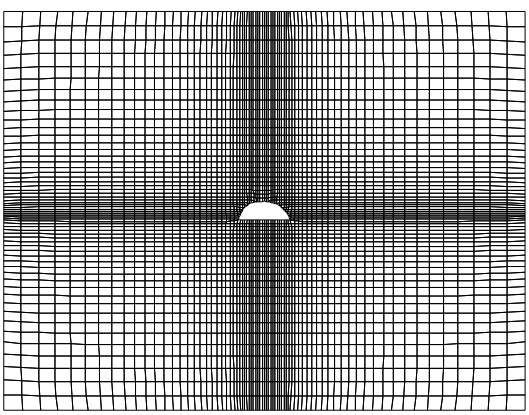

Figure 5. Layout of numerical grid for displacement and error calculations

Table 4 summarizes the calibrated geotechnical parameters obtained using the FDM–GA algorithm, along with the corresponding objective function error values and calculated convergence values from 30 independent optimization runs. Each run required approximately 12 to 24 hours on an Intel Core i9-9900K processor. The differences in runtime are mainly due to the random generation of the initial chromosome population and the stochastic nature of the mutation process. The consistently low objective function error values demonstrate the robustness and repeatability of the proposed algorithm in calibrating geotechnical parameters for a complex real-world tunnelling problem.

The ranges of the calibrated geotechnical parameters obtained from the 30 optimized models, as presented in Table 4, are summarized under the "Back analyzed range" column in Table 3. A comparison between these back analyzed ranges and the initially assumed search ranges in Table 3 shows that the calibrated ranges for density (ρ), Poisson's ratio (υ), and friction angle (φ) remain largely unchanged. In contrast, the range of the coefficient of lateral earth pressure at rest (K_0) is moderately reduced. Finally, the ranges of Young's modulus (E) and cohesion (c) are considerably narrowed following calibration. Notably, the preliminary values of E and c used to generate the initial LDP and GRC curves fall outside the corresponding calibrated ranges. This observation indicates that the initial estimates of tunnel deformation and stress relaxation, derived from the original LDP and GRC curves, should be re-evaluated using the calibrated parameter values.

Although some calibrated parameters exhibit limited variability, the parameter ranges remain relatively broad. Therefore, it is essential to identify the parameter set that best represents the geotechnical properties of the Hezar Darreh Formation through which the Pardis Highway Tunnel passes. The reported geotechnical properties of conglomerate formations from other tunnel and underground excavation projects, as summarized in Table 2, provide an independent basis for interpreting the calibrated models presented in Table 4 and selecting a representative and geologically consistent parameter set for the back analysis problem. As discussed for verification examples in Part I, this interpretation can be strengthened by examining the inter-parameter correlations among the calibrated models. Accordingly, an analysis of the relationships between different pairs of calibrated parameters identified two linear correlations (Figure 6): one between cohesion (c) and friction angle (φ), and the other between Young's modulus (E) and the coefficient of lateral earth pressure at rest (K_0).

$$\varphi = -0.1823\, c + 36.794 \quad (R^2 = 0.9609) \tag{1}$$

$$K_0 = 1.8022\, E + 0.8964 \quad (R^2 = 0.5747) \tag{2}$$

Where are:

φ – friction angle (°),

c – cohesion (kPa),

K_0 – coefficient of lateral earth pressure at rest,

E – Young's modulus (GPa).

Applying the reported parameter ranges from Table 2 to Figure 6 indicates that only Project No. 1 (Tehran Metro Tunnels) and Project No. 4 (Resalat Tunnel) are consistent with the calibrated ranges of cohesion (c), friction angle (φ), Young's modulus (E), and the coefficient of lateral earth pressure at rest (K_0). The remaining projects show significant deviations from these calibrated ranges. Notably, Project No. 2 corresponds to the Pardis Tunnel and contains geotechnical parameters derived from preliminary site investigations. Except for the friction angle (φ), the estimated values of cohesion (c) and Young's modulus (E) fall outside the calibrated ranges, suggesting that the preliminary estimates may not adequately represent the in-situ rock mass properties. Projects No. 3, 5, and 6 are associated with deep underground structures, such as caverns and water conveyance tunnels. They are therefore likely to have been excavated in stronger rock masse formations than those encountered at the Pardis tunnel site. Consequently, only Projects No. 1 and 4, both representing shallow transportation tunnels excavated in comparable conglomerate formations, are considered the most appropriate engineering analogues for interpreting the calibrated parameter sets of the Pardis Highway Tunnel.

Based on the fitted trendline in Figure 6a and the cohesion (c) and friction angle (φ) values reported for Projects No. 1 and 4, a representative cohesion value of 21 kPa was selected, as it is consistent with both reference projects. According to the fitted c–φ correlation in Figure 6a, this value corresponds to a friction angle of 33°, represented by the yellow asterisk in Figure 6a. Although this value falls within the range reported for Project No. 4, it is slightly lower than the 37° reported for Project No. 1.

Table 4. Summary of estimated ground geotechnical parameters along with the relevant error and convergence values for tunnel no. 1, Pardis Highway project

Model No.	ρ (kg/m^3)	E (GPa)	υ	c (kPa)	φ (°)	K_0	Error	TL_c (mm)	TR_c (mm)	LR_c (mm)
1	2265	0.8127	0.3202	50.48	26.40	2.608	3.438×10^{-4}	7.270	6.908	15.47
2	2531	1.1280	0.3171	33.65	30.64	2.966	5.258×10^{-5}	7.168	6.513	15.54
3	2173	0.6673	0.3619	38.53	29.25	2.369	3.150×10^{-5}	7.246	6.623	15.53
4	2359	0.7388	0.3970	41.30	29.37	2.738	5.775×10^{-5}	7.294	6.476	15.36
5	2553	0.6317	0.2607	90.38	21.69	1.721	3.989×10^{-5}	7.187	6.662	15.41
6	2366	0.7685	0.3843	27.56	32.26	2.458	1.093×10^{-4}	7.331	6.685	15.57
7	2326	0.7372	0.3422	19.68	33.69	2.234	8.585×10^{-5}	7.389	6.658	15.42
8	2449	1.0170	0.2561	89.94	21.51	2.742	3.226×10^{-4}	6.973	6.395	15.49
9	2499	0.6000	0.2816	59.52	25.76	1.628	4.394×10^{-6}	7.271	6.544	15.43
10	2362	0.7568	0.3892	28.88	31.95	2.447	8.138×10^{-5}	7.306	6.722	15.48
11	2684	0.9410	0.3017	95.65	20.22	2.109	1.663×10^{-4}	7.044	6.625	15.55
12	2396	0.5990	0.3128	94.72	20.23	1.849	5.960×10^{-5}	7.111	6.591	15.43
13	2147	0.4938	0.3259	44.12	27.45	1.728	1.210×10^{-4}	7.435	6.502	15.47
14	2149	0.8219	0.2892	78.47	21.70	2.771	1.798×10^{-4}	7.433	6.691	15.55
15	2178	0.4374	0.3317	56.46	24.87	1.508	1.328×10^{-4}	7.185	6.387	15.36
16	2270	0.9969	0.2609	41.08	27.85	2.907	4.074×10^{-4}	7.134	6.864	15.64
17	2373	0.7395	0.3801	95.58	20.50	2.667	5.253×10^{-5}	7.334	6.669	15.47
18	2261	0.8193	0.3226	26.34	31.92	2.422	1.324×10^{-5}	7.302	6.550	15.48
19	2541	0.9766	0.3533	8.418	36.76	2.612	5.779×10^{-4}	7.640	6.387	15.37
20	2525	0.9853	0.2797	43.53	28.85	2.491	9.859×10^{-5}	7.083	6.533	15.51
21	2286	0.8213	0.3092	23.72	32.47	2.352	3.380×10^{-4}	7.540	6.670	15.58
22	2440	0.8159	0.3026	59.69	25.80	2.353	4.170×10^{-4}	7.168	6.853	15.68
23	2176	0.6987	0.3290	62.17	23.62	2.373	5.758×10^{-5}	7.246	6.683	15.53
24	2385	0.8130	0.3188	17.32	34.26	2.280	2.299×10^{-6}	7.272	6.566	15.46
25	2624	0.9731	0.3171	11.66	35.86	2.404	3.108×10^{-5}	7.279	6.479	15.48
26	2461	1.0060	0.2535	80.45	21.00	2.296	5.213×10^{-4}	7.456	6.922	15.53
27	2441	0.8882	0.2942	65.10	24.24	2.450	7.070×10^{-5}	7.120	6.651	15.41
28	2551	0.6631	0.3649	73.07	24.96	2.102	6.808×10^{-5}	7.351	6.625	15.54
29	2481	0.6425	0.2687	31.44	30.44	1.653	1.440×10^{-4}	7.406	6.462	15.34
30	2184	0.8596	0.2597	75.10	21.80	2.637	1.245×10^{-6}	7.203	6.528	15.46

TL_c: Calculated convergence along the Top-Left direction
TR_c: Calculated convergence along the Top-Right direction
LR_c: Calculated convergence along the Left-Right direction

As presented in Table 2, the only additional geotechnical parameter available for comparison is Young's modulus (E), for which the maximum reported value is 0.15 GPa. However, Figure 6b shows that the calibrated Young's modulus values are generally higher, and the available reference data do not permit an independent determination of E or K_0. Among the calibrated models listed in Table 4, Model No. 15 exhibits the lowest Young's modulus (0.44 GPa), making it the closest match to the values reported for the comparable projects. Based on Equation (2), this value corresponds to a K_0 value of 1.69.

A review of Table 2 shows that the parameters ρ and υ were not reported for Projects No. 1 and 4. Furthermore, the plots in Figure 6 do not reveal any clear correlation between these parameters and the calibrated values of c, φ, E, and K_0. To estimate appropriate values for ρ and υ, the FDM–GA algorithm was re-executed while keeping the calibrated values of c, φ, E, and K_0 fixed, as determined from the preceding analyses. The results of three independent optimization runs are summarized in Table 5. As shown, the estimated values of ρ and υ, together with their corresponding error values, exhibit very little variation among the three runs. Figure 7 illustrates the convergence histories of the optimization process for each run. Although the three optimizations followed different evolutionary paths, they all converged to nearly identical parameter values and objective function error values. These findings support two important conclusions: First, when c, φ, E, and K_0 are fixed, the back analysis of ρ and υ produces essentially unique and consistent solutions. Second, the close agreement among the independent optimization runs demonstrates the stability, repeatability, and reliability of the integrated FDM–GA framework.

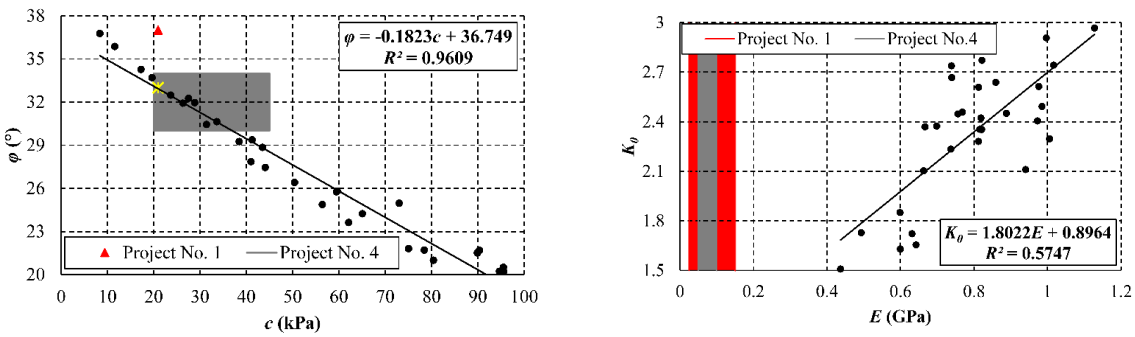

(a) (b)

Figure 6. Inter-parameter correlations between the calibrated parameters: (a) cohesion (c) – friction angle (φ) and (b) Young's modulus (E) – coefficient of lateral earth pressure at rest (K_0) correlations

Table 5. Summary of estimated values for density (ρ) and Poisson's ratio (υ) from three independent runs of the integrated FDM-GA algorithm with fixed c, φ, E, and K_0 values

Run No.	ρ (kg/m³)	υ	error
1	2303	0.3980	3.476×10^{-4}
2	2326	0.3992	3.502×10^{-4}
3	2322	0.3996	3.676×10^{-4}

Based on the results summarized in Table 5, the values of ρ = 2300 kg/m³ and υ = 0.40 were selected. The complete set of calibrated geotechnical parameters is presented in the final column of Table 3. Using these input values, the final calculated convergence values are TL_c = 7.341 mm, TR_c = 6.604 mm, and LR_c = 15.12 mm, corresponding to a total relative error of 3.476×10^{-4}. Although some parameter sets listed in Table 4 produce slightly lower objective function error values, the optimization results presented in Part I and the analyses in the present study demonstrate that minimizing the numerical error alone does not necessarily lead to the most representative engineering parameters. Instead, the preferred parameter set is the one that simultaneously satisfies the field monitoring data, the optimization results, the observed inter-parameter correlations, and the available independent geotechnical evidence.

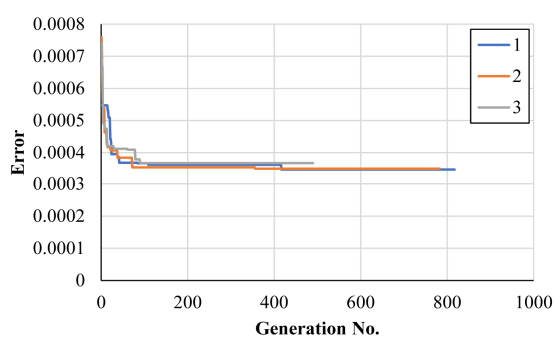

Figure 7. Error evolution curves for three independent runs of the integrated FDM-GA algorithm during the back analysis of ρ and υ with fixed values of c, φ, E, and K_0

4. The Effect of Initial Stress Relaxation Factor on the Back Analysis Results

Neither the tunnel support system nor the monitoring instrumentation can be installed exactly at the tunnel face. Moreover, ground deformation and stress relaxation begin ahead of the advancing excavation face. Consequently, a significant portion of the tunnel deformation occurs before the installation of the support system and the monitoring instrumentation. Since the monitoring system records only the deformations that occur after installation, the pre-installation deformation must be excluded when comparing measured and numerically predicted convergence values. In 3D numerical models, this adjustment can be achieved directly by explicitly modelling the distance between the tunnel face and the locations where the support system and monitoring instrumentation are installed. However, because back analysis requires a large number of repeated numerical simulations, the use of 3D models becomes computationally expensive. Therefore, 2D plane strain models are commonly adopted for practical tunnel back analysis.

In 2D models, the deformation and stress relaxation occurring before the installation of the support system or monitoring instrumentation must be represented indirectly. The standard, and widely accepted, approach is to estimate these quantities using LDP and GRC curves, as illustrated in Figure 4. However, constructing the LDP and GRC requires the geotechnical parameters of the rock mass, which are the unknown variables in the back analysis problem. Consequently, the initial LDP and GRC curves presented in Section 3 were generated using the mean values of the assumed parameter ranges listed in Table 3 to provide preliminary estimates of the pre-installation deformation and the corresponding stress relaxation factor.

Following parameter calibration, it became evident that several of the calibrated geotechnical parameters differed substantially from their initially assumed values (Table 3). Accordingly, the LDP and GRC curves were recalculated using the calibrated parameter set, and the updated curves are presented in Figure 8. The revised analysis yielded a stress relaxation factor of 85%, representing an increase of 1.5 percentage points compared with the preliminary estimate. Although this difference appears small, its influence on the back analysis results is substantial. As shown in Table 6, increasing the stress relaxation factor by only 1.5 percentage points increased the objective function error by approximately a factor of 77. This finding demonstrates the high sensitivity of tunnel back analysis to the assumed stress relaxation factor. Consequently, the FDM–GA optimization was repeated using the corrected stress relaxation factor to evaluate its influence on the calibrated geotechnical parameters.

To evaluate the sensitivity of the back analysis results to the assumed stress relaxation factor, the stress relaxation factor was increased from 83.5% to 85% before the monitoring points were activated. Following this adjustment, 30 independent FDM–GA optimization runs were performed to obtain a revised set of calibrated geotechnical parameters. The resulting calibrated parameter sets, together with their corresponding error values and calculated convergence values, are summarized in Table 7.

To identify the representative geotechnical parameter set that best satisfies the available geotechnical evidence, the correlations between cohesion (c) and friction angle (φ), and between Young's modulus (E) and the coefficient of lateral earth pressure at rest (K_0), were re-evaluated using the calibrated results presented in Table 7. The updated correlations are shown in Figure 9. For comparison, the corresponding trendlines from Figure 6 are superimposed as light grey lines, whereas the updated trendlines are shown in black. This comparison illustrates the influence of the revised LDP and GRC estimates, resulting from the updated stress relaxation factor, on the calibrated parameter relationships. As shown, the revised c–φ and E–K_0 relationships remain approximately linear and are represented by the following equations:

$$\varphi = -0.1781\, c + 35.842 \quad (R^2 = 0.9391) \tag{3}$$

$$K_0 = 2.5665\, E + 0.2912 \quad (R^2 = 0.7728) \tag{4}$$

Where are:

φ – friction angle (°),

c – cohesion (kPa),

K_0 – coefficient of lateral earth pressure at rest,

E – Young's modulus (GPa).

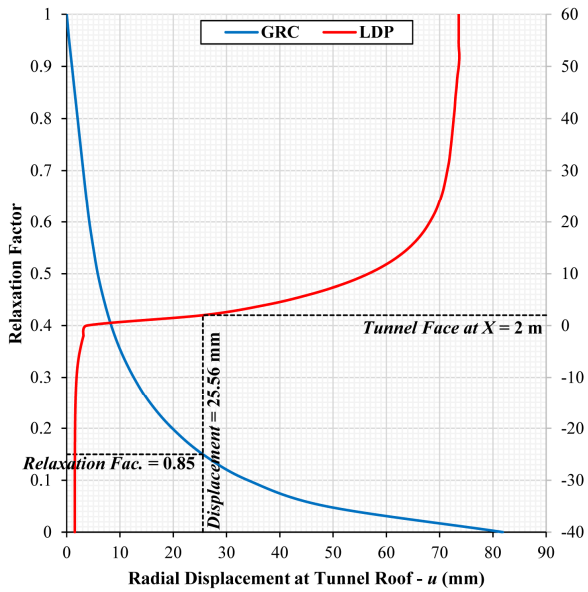

Figure 8. Corrected LDP and GRC curves for calculating the displacement and stress relaxation values before the installation of the instrumentation system

In Figure 9a, the corrected c–φ trendline is nearly parallel to the initial trendline, derived from the preliminary LDP and GRC curves, but is shifted slightly downward. This indicates that the revised stress relaxation factor has little influence on the fundamental relationship between the shear strength parameters. Instead, it systematically shifts the calibrated solutions toward lower values of cohesion and/or friction angle. In other words, underestimating the stress relaxation factor during the initial LDP and GRC estimation may lead to an overestimation of the shear strength parameters obtained from 2D back analysis. Such overestimation may result in non-conservative estimates of rock mass strength and, consequently, unconservative tunnel support designs if the calibrated parameters are adopted without accounting for the effects of stress relaxation.

In contrast, the updated E–K_0 trendline (shown as the black line in Figure 9b) exhibits a more pronounced change. Compared with the initial trendline, the updated correlation is rotated, indicating that the relationship between Young's modulus (E) and the coefficient of lateral earth pressure at rest (K_0) is more sensitive to changes in the assumed stress relaxation factor. Consequently, corrections to the stress relaxation factor may lead to either higher or lower calibrated values of E or K_0, depending on the corresponding variation of the other parameter. Unlike the c–φ relationship, which is primarily shifted while maintaining a similar slope, the E–K_0 correlation undergoes a noticeable change in both slope and position. This behavior indicates that the assumed stress relaxation factor significantly affects the interaction between deformation stiffness and in-situ stress conditions. Therefore, this factor must be carefully considered during parameter calibration. Following the procedure described in the previous section, the cohesion value reported for Projects No. 1 and 4 (Table 2) was fixed at 21 kPa. Using Equation (3), the corresponding friction angle was recalculated as φ = 32°, representing approximately a 3% decrease from the previously estimated value of 33°. Conversely, if the friction angle is fixed at 33°, Equation (3) yields an updated cohesion value of 16 kPa, corresponding to a considerably larger decrease of approximately 24% relative to the original value of 21 kPa. For the estimation of K_0, the minimum calibrated value of Young's modulus from Table 7 (approximately 0.44 GPa) was substituted into Equation (4), resulting in $K_0 = 1.42$, which represents a reduction of approximately 16% compared with the previous estimate. These results indicate that the friction angle is only weakly affected by changes in the assumed stress relaxation factor, whereas cohesion and the coefficient of lateral earth pressure at rest exhibit substantially greater sensitivity. This finding demonstrates that inaccuracies in estimating the stress relaxation factor can introduce significant bias into the calibrated geotechnical parameters and therefore should not be regarded as a secondary modelling assumption in 2D tunnel back analysis.

Table 6. Measured and calculated convergence values based on initial and corrected stress relaxation factors

	Measured Values	Calculated values with 1st back analysis estimations	Calculated with 1st back analysis estimations and corrected stress relaxation factor
TL (mm)	7.247	7.341	5.482
TR (mm)	6.571	6.604	4.329
LR (mm)	15.443	15.12	14.53
Error	0	3.476×10^{-4}	2.687×10^{-2}

Table 7. Summary of calibrated geotechnical parameters obtained from 30 FDM-GA optimization runs with the corrected stress relaxation factor of 85% prior to measurement points activation

Model No.	ρ (kg/m^3)	E (GPa)	υ	c (kPa)	φ (°)	K_0	Error	TL_c (mm)	TR_c (mm)	LR_c (mm)
1	2555	0.7372	0.3033	19.68	33.39	2.025	2.328×10^{-4}	7.377	6.326	15.42
2	2444	0.7235	0.3126	19.68	33.25	2.083	2.062×10^{-4}	7.498	6.501	15.41
3	2459	0.5299	0.3372	79.03	21.97	1.785	9.016×10^{-5}	7.315	6.651	15.58
4	2364	0.8657	0.2995	70.32	22.89	2.750	1.009×10^{-4}	7.144	6.437	15.37
5	2135	0.4362	0.2938	65.30	22.37	1.598	2.752×10^{-5}	7.257	6.485	15.40
6	2359	0.8731	0.3097	73.99	20.13	2.200	2.449×10^{-4}	7.291	6.795	15.62
7	2633	0.9520	0.3369	40.26	28.97	2.925	3.538×10^{-4}	7.091	6.781	15.76
8	2327	0.9060	0.2523	51.40	25.11	2.489	2.158×10^{-4}	7.007	6.659	15.36
9	2199	0.5701	0.2525	46.31	26.38	1.853	1.553×10^{-4}	7.270	6.730	15.61
10	2689	0.4999	0.3271	94.26	20.11	1.354	4.281×10^{-5}	7.320	6.484	15.41
11	2615	0.9923	0.3232	84.35	22.52	2.924	6.676×10^{-5}	7.387	6.623	15.44
12	2305	0.4478	0.2694	7.608	33.74	1.037	4.520×10^{-4}	7.517	6.317	15.56
13	2107	0.6859	0.3102	13.92	34.22	2.283	4.955×10^{-4}	7.602	6.454	15.61
14	2693	0.6781	0.2097	26.24	31.64	1.727	6.518×10^{-3}	7.526	6.394	16.88
15	2161	0.8537	0.3127	28.09	30.12	2.867	5.314×10^{-4}	7.277	6.989	15.49
16	2508	1.0330	0.2960	35.44	29.50	2.799	4.994×10^{-4}	7.015	6.868	15.29
17	2659	0.6268	0.3990	34.10	31.08	2.030	6.176×10^{-4}	7.642	6.654	15.65
18	2208	0.5783	0.3377	48.53	26.43	2.165	3.970×10^{-4}	7.024	6.773	15.65
19	2688	0.7218	0.3638	55.69	27.18	2.262	1.127×10^{-4}	7.269	6.761	15.41
20	2488	0.5234	0.3891	63.06	25.27	1.857	4.448×10^{-5}	7.184	6.516	15.54
21	2624	0.8274	0.3114	83.79	20.63	2.055	8.274×10^{-4}	7.345	6.983	15.76
22	2644	0.9045	0.3508	95.19	20.51	2.686	9.427×10^{-4}	7.368	6.887	15.89
23	2308	0.5940	0.3591	59.24	24.62	2.236	3.949×10^{-4}	7.043	6.280	15.37
24	2596	0.4618	0.3617	62.19	24.59	1.415	1.171×10^{-4}	7.404	6.468	15.51
25	2254	0.5530	0.2982	61.65	23.73	1.883	4.484×10^{-4}	7.017	6.770	15.69
26	2525	0.5786	0.2917	39.30	28.43	1.592	7.243×10^{-5}	7.390	6.576	15.51
27	2619	0.8645	0.3175	50.43	27.11	2.533	3.711×10^{-4}	7.276	6.891	15.59
28	2601	0.7072	0.3300	34.24	30.63	2.015	8.050×10^{-5}	7.313	6.440	15.37
29	2519	0.5339	0.2529	23.60	30.44	1.187	1.991×10^{-4}	7.306	6.350	15.56
30	2674	0.8221	0.3335	33.10	31.11	2.225	2.398×10^{-4}	7.310	6.466	15.19

To estimate the values of density (ρ) and Poisson's ratio (υ), the FDM–GA algorithm was executed in three independent optimization runs using the fixed input parameters c = 21 kPa, φ = 32°, E = 0.44 GPa, and K_0 = 1.42. The optimization yielded average values of ρ = 2600 kg/m³ and υ = 0.40. Compared with the previous calibration, the estimated value of Poisson's ratio remained unchanged, indicating that υ exhibits negligible sensitivity to variations in the assumed stress relaxation factor within the investigated range. In contrast, the estimated density increased by approximately 12%, suggesting a moderate sensitivity of ρ to the stress relaxation assumption. These results indicate that the influence of stress relaxation is parameter-dependent, with density exhibiting a measurable response. In contrast, Poisson's ratio remains essentially unaffected under the conditions considered in this study.

The full set of calibrated geotechnical parameters, updated to account for the revised stress relaxation factor, is presented in Table 8. For comparison, the corresponding results obtained using the preliminary stress relaxation factor are also included. Using the revised parameter set, the calculated convergence values are TL_c = 7.131 mm, TR_c = 6.786 mm, and LR_c = 15.13 mm, corresponding to a total relative error of 4.773×10^{-4}. Although the revised calibration yields a slightly higher objective function error than the preliminary solution, it provides a more physically representative engineering parameter set because it is based on an improved estimate of the stress relaxation factor.

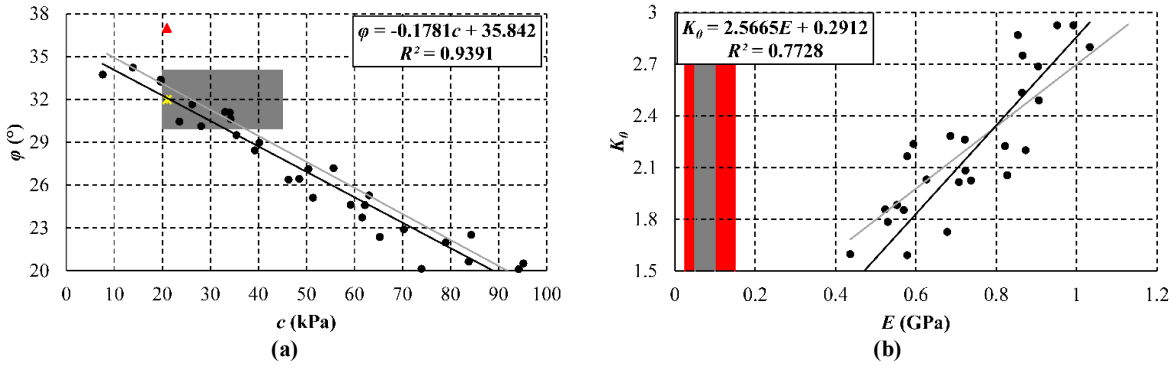

Figure 9. Updated inter-parameter correlations for the calibrated model results in Table 10 after correcting the stress relaxation factor: (a) c–φ relationship and (b) E–K_0 relationship

Table 8. Final set of back-calculated geotechnical parameters after correction of the stress relaxation factor and stress relaxation rate, compared with the preliminary back analysis results

	Preliminary back analysis results	The results after the correction of stress relaxation factor	The results after the correction of the stress relaxation rate
mass density – ρ (kg/m^3)	2300	2600	2600
Young's modulus – E (GPa)	0.44	0.44	0.44
Poisson's ratio – υ	0.40	0.40	0.40
cohesion – c (kPa)	21	21 (16)	21
friction angle – φ (°)	33	32 (33)	33
K_0 ratio	1.69	1.42	1.48
TL_c (mm)	7.341	7.131	7.158
TR_c (mm)	6.604	6.786	6.222
LR_c (mm)	15.12	15.13	15.61
Error	3.476×10^{-4}	4.773×10^{-4}	4.685×10^{-4}

5. The Effect of Stress Relaxation Rate on the Back Analysis Results

The mechanical response of ground materials is strongly influenced by their stress history and the stress path changes that occur during excavation. In numerical analyses of underground structures, accurately reproducing the construction sequence is therefore essential, because the stress path governs the mobilized strength, deformation characteristics, and failure mechanisms of the ground [25, 26]. This aspect is particularly important in tunneling, where stress redistribution develops progressively as the excavation face advances, producing spatially and temporally varying ground responses. Previous studies have shown that neglecting intermediate excavation stages may alter the stress field and produce irreversible plastic deformations that persist throughout the excavation process and into the final equilibrium state [27, 28]. The findings of the present study further demonstrate that this progressive stress redistribution cannot be neglected in tunnel back analysis. In 2D tunnel analyses, the effects of 3D excavation are commonly represented through the stress relaxation factor derived from the LDP and GRC. The stress relaxation is also influenced by the excavation procedure adopted in the numerical model, particularly the excavation advance length (or excavation step size). Previous studies have shown that smaller excavation steps provide a more realistic representation of stress redistribution ahead of the tunnel face. In contrast, larger steps may overestimate stress concentrations and underestimate ground relaxation [29, 30]. Consequently, the selection of excavation step size affects not only the predicted LDP but also the stress relaxation factor subsequently used in 2D back analysis. In weak or highly fractured rock masses, these effects may become even more pronounced because excavation advance interacts with time-dependent processes such as creep and stress relaxation [30]. Therefore, accurate representation of the excavation sequence is an essential prerequisite for reliable geotechnical parameter calibration using 2D inverse analysis frameworks.

In the back analysis procedure presented in the preceding sections, stress relaxation in the 2D numerical model was implemented in two stages:

1. An initial stress relaxation stage before the installation of the tunnel support system and convergence monitoring pins. This stage was introduced to simulate the ground deformation

occurring prior to the installation of the support system and monitoring instrumentation.

2. A second stress relaxation stage was introduced after the installation of the support system and convergence monitoring pins, during which the calculated convergence values were obtained for comparison with the field measurements.

To investigate the influence of the stress relaxation rate (representing the excavation advance process) on the back analysis results, an additional numerical simulation was conducted. In this simulation, the stress relaxation was introduced in 12 equal incremental stages, with 8.33% of the in-situ stress released during each stage, thereby simulating a gradual excavation process. To ensure a direct comparison with the reference case, the total stress relaxation factor applied before the installation of the tunnel support system and monitoring instrumentation was kept constant at 83.5%, as established in Section 3. Accordingly, only the rate of stress relaxation was modified, while the total pre-installation stress relaxation remained unchanged.

Following the methodology adopted in the previous analyses, a series of 30 independent FDM–GA optimization runs was conducted. During these analyses, the stress relaxation process was implemented in 12 equal incremental stages, resulting in a revised set of calibrated geotechnical parameters. The calibrated parameter sets obtained from the optimization runs are summarized in Table 9. To identify the representative engineering parameters, the relationships between cohesion (c) and friction angle (φ), and between Young's modulus (E) and the coefficient of lateral earth pressure at rest (K_0), were re-evaluated using the calibrated results. The resulting relationships are presented in Figure 10, where the corresponding trendlines from the preliminary back analysis (Section 2) are included as light grey lines for comparison. The equations below illustrate the resulting linear relationships:

$$\varphi = -0.1708\, c + 36.432 \quad (R2 = 0.9576) \tag{5}$$

$$K_0 = 2.4429\, E + 0.4013 \quad (R2 = 0.7548) \tag{6}$$

Where are:

φ – friction angle,

c – cohesion,

K_0 – coefficient of lateral earth pressure at rest,

E – Young's modulus.

The updated c–φ correlation exhibits only a negligible deviation from that obtained using the instantaneous two-step stress relaxation procedure. This indicates that the stress relaxation rate has little influence on the calibrated shear strength parameters, namely cohesion (c) and friction angle (φ). In contrast, the correlation between Young's modulus (E) and the coefficient of lateral earth pressure at rest (K_0) shows a more pronounced change, indicating that the calibrated deformation-related parameters are considerably more sensitive to the stress relaxation rate. A comparison with Figure 9b further shows that the influence of the stress relaxation rate on the E–K_0 relationship is broadly similar to that produced by changes in the initial stress relaxation factor. This finding suggests that both the magnitude and the rate of stress relaxation primarily affect the stiffness–stress relationship, whereas the shear strength relationship remains comparatively stable.

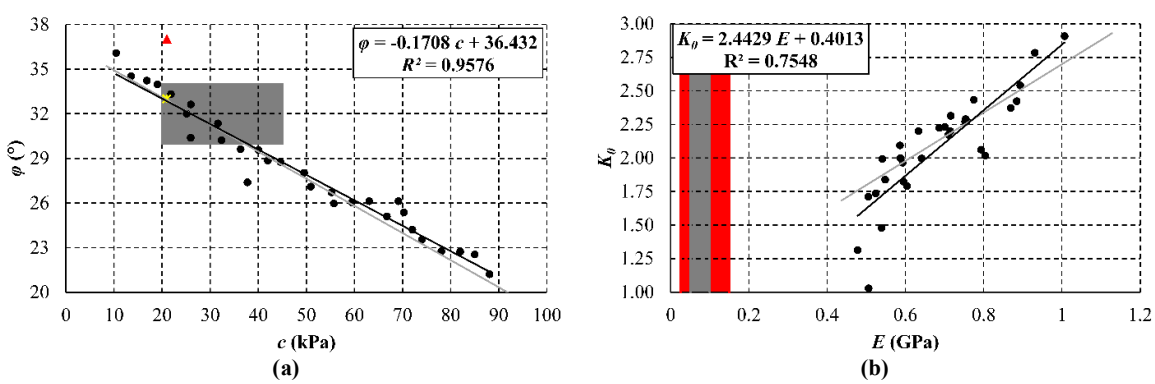

Figure 10. Updated inter-parameter correlations for the calibrated model results in Table 12 after correcting the stress relaxation rate: (a) c–φ relationship and (b) E–K_0 relationship

Table 9. Summary of calibrated geotechnical parameters obtained from 30 FDM-GA optimization runs with the corrected stress relaxation rate

Model No.	ρ (kg/m^3)	E (GPa)	υ	c (kPa)	φ (°)	K_0	Error	TL_c (mm)	TR_c (mm)	LR_c (mm)
1	2426	0.5488	0.3439	66.79	25.10	1.837	2.454×10^{-5}	7.237	6.597	15.53
2	2500	0.7538	0.3771	26.04	32.62	2.288	6.632×10^{-5}	7.195	6.710	15.45
3	2249	0.7103	0.2910	36.38	29.61	2.172	6.852×10^{-5}	7.343	6.688	15.46
4	2660	0.5397	0.3148	59.54	26.04	1.477	1.861×10^{-4}	7.480	6.643	15.50
5	2164	0.6337	0.3381	55.75	25.96	2.199	1.577×10^{-4}	7.306	6.760	15.56
6	2364	0.7937	0.2610	88.14	21.20	2.061	2.237×10^{-4}	7.039	6.748	15.47
7	2393	0.7161	0.3853	19.08	33.96	2.313	8.359×10^{-5}	7.238	6.737	15.42
8	2618	0.8043	0.2512	63.12	26.12	2.017	1.023×10^{-4}	7.343	6.729	15.44
9	2501	0.8848	0.3286	21.87	33.31	2.422	3.090×10^{-5}	7.344	6.586	15.47
10	2344	0.6868	0.3602	44.67	28.75	2.223	9.590×10^{-5}	7.124	6.443	15.42
11	2544	0.5063	0.2823	37.78	27.38	1.028	5.033×10^{-5}	7.291	6.449	15.44
12	2352	0.7008	0.3583	40.06	29.57	2.231	6.835×10^{-5}	7.120	6.508	15.39
13	2270	1.007	0.2821	82.05	22.72	2.907	5.931×10^{-5}	7.172	6.688	15.47
14	2254	0.5872	0.3484	25.13	31.99	1.999	6.457×10^{-5}	7.372	6.648	15.44
15	2425	0.5956	0.2965	55.27	26.70	1.823	1.290×10^{-4}	7.151	6.389	15.42
16	2699	0.6423	0.3962	69.20	26.12	1.995	7.253×10^{-5}	7.362	6.676	15.45
17	2472	0.8936	0.3467	10.47	36.08	2.540	1.813×10^{-4}	7.486	6.630	15.45
18	2165	0.5412	0.3693	13.59	34.51	1.993	6.069×10^{-5}	7.302	6.483	15.54
19	2405	0.4778	0.3506	26.00	30.39	1.312	1.539×10^{-4}	7.418	6.535	15.59
20	2393	0.7753	0.3855	31.65	31.34	2.432	8.665×10^{-5}	7.087	6.584	15.39
21	2552	0.6041	0.3206	49.57	28.02	1.790	1.079×10^{-4}	7.402	6.542	15.35
22	2266	0.5865	0.3875	74.13	23.54	2.093	7.206×10^{-5}	7.149	6.644	15.35
23	2536	0.7154	0.3794	70.34	25.37	2.198	6.230×10^{-5}	7.286	6.701	15.50
24	2209	0.9310	0.2839	78.10	22.75	2.783	7.334×10^{-5}	7.104	6.628	15.42
25	2488	0.5248	0.3350	85.05	22.54	1.736	1.276×10^{-4}	7.416	6.664	15.52
26	2337	0.7529	0.3216	16.87	34.22	2.270	5.896×10^{-6}	7.217	6.541	15.43
27	2219	0.5934	0.3099	32.43	30.22	1.964	3.636×10^{-5}	7.343	6.536	15.40
28	2307	0.7574	0.3128	42.04	28.84	2.275	1.675×10^{-5}	7.231	6.644	15.44
29	2321	0.8701	0.2692	50.95	27.10	2.372	3.388×10^{-5}	7.200	6.666	15.45
30	2455	0.5051	0.3529	72.10	24.21	1.710	2.391×10^{-5}	7.173	6.549	15.40

Substituting c = 21 kPa into Equation (5) and E = 0.44 GPa into Equation (6) yields φ = 33° (32.8°) and K_0 = 1.48. Using these values as fixed inputs, the FDM–GA optimization was subsequently performed to estimate the density (ρ) and Poisson's ratio (υ), resulting in ρ = 2600 kg/m³ and υ = 0.40. These results indicate that the influence of the stress relaxation rate on ρ and υ is comparable to that of the initial stress relaxation factor discussed in Section 4. The complete set of calibrated geotechnical parameters, together with the calculated convergence values (TL_c, TR_c, and LR_c) and the corresponding objective function errors, is summarized in Table 8. Comparison with the preliminary back analysis results indicates that incorporating the stress relaxation rate primarily modifies the calibrated value of K_0. However, correcting the initial stress relaxation factor affects both K_0 and, to a lesser extent, the shear strength parameters (c and φ). This comparison demonstrates that the initial stress relaxation factor exerts a broader influence on parameter calibration. In contrast, the stress relaxation rate mainly affects parameters associated with the in-situ stress state.

Figure 11 compares the effects of the initial stress relaxation factor and the stress relaxation rate on the relationships between c–φ and E–K_0 obtained from the calibrated models. As illustrated in Figure 11a, the c–φ correlation derived from the preliminary back analysis results (black line) is influenced by both corrections, although in different ways. The initial stress relaxation factor correction (blue line) primarily translates the correlation downward, indicating systematically lower calibrated shear strength parameters. In contrast, the stress relaxation rate correction (red line) rotates the trendline, indicating that its influence depends on the magnitude of cohesion. At higher cohesion values, the calibrated friction angle, and consequently the estimated shear strength, increase slightly, whereas the effect becomes negligible at lower cohesion values.

The E–K_0 correlation (Figure 11b) exhibits a broadly similar response to both corrections. In both cases, the trendlines rotate about approximately the same pivot point ($E \approx 0.8$ GPa). Consequently, for E values below approximately 0.8 GPa, both corrections decrease the calibrated

K_0 value, whereas for higher E values they increase it. Moreover, the magnitude of this effect becomes more pronounced as E deviates further from the pivot point. A closer examination shows that the trendline corresponding to the initial stress relaxation factor correction (blue line) is slightly steeper than that associated with the stress relaxation rate correction (red line), indicating a somewhat stronger influence of the initial stress relaxation factor on the E–K_0 relationship.

Overall, Figure 11 demonstrates that the two stress relaxation variables influence the calibrated parameter relationships in different ways. The initial stress relaxation factor primarily affects the absolute values of the calibrated parameters, whereas the stress relaxation rate mainly modifies the parameter correlations through changes in their relative interaction. For the Pardis Highway Tunnel case, the calibration results are therefore somewhat more sensitive to the initial stress relaxation factor than to the stress relaxation rate, highlighting the importance of accurately estimating pre-support stress release in 2D tunnel back analysis.

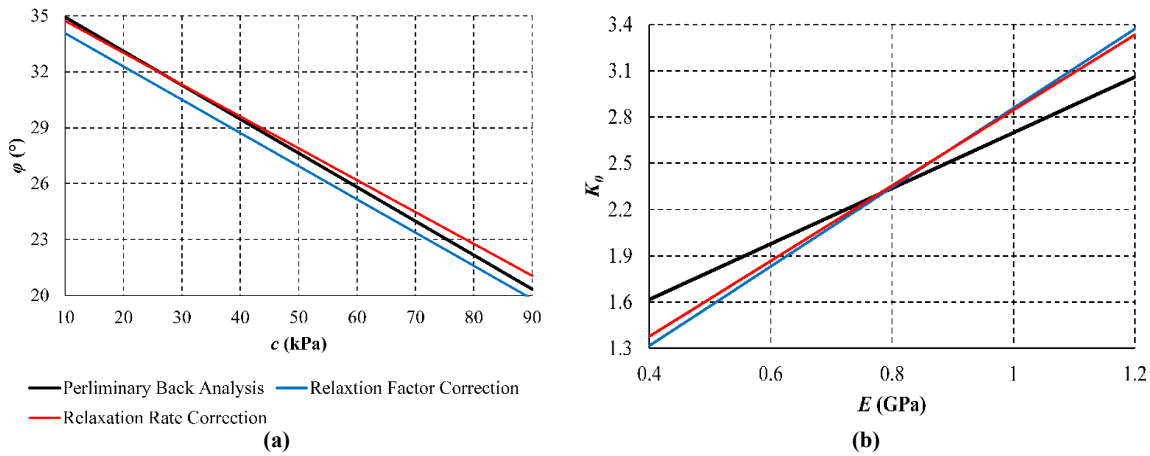

Figure 11. Comparison of the effects of stress relaxation factor and stress relaxation rate corrections on the (a) c – φ and (b) E – K_0 correlations among the calibrated models

As summarized in Table 8, incorporating both the stress relaxation factor and stress relaxation rate corrections resulted in the same representative calibrated geotechnical parameters: ρ = 2600 kg/m³, E = 0.44 GPa, υ = 0.40, c = 21 kPa, and φ = 33°. With these parameters fixed, the final model calibration yielded K_0 = 1.73 and a minimum objective function error of 1.305×10^{-4}. The agreement of the calibrated parameters obtained from the two correction procedures demonstrates the consistency and robustness of the proposed calibration methodology.

To assess the engineering implications of these corrections, the distributions of ground displacement and plastic zones, as well as the axial forces and bending moments in the support elements, are compared as illustrated in Figure 12. The figure contrasts the preliminary back analysis model (left column) with the model incorporating both the stress relaxation factor and stress relaxation rate corrections (right column). Only minor differences were observed in the displacement distributions and the extent of the plastic zones between the two cases. Similarly, the corrected model produced maximum axial forces and bending moments approximately 3% lower than those obtained from the preliminary calibration. These relatively small differences indicate that, although stress relaxation corrections noticeably influence the calibrated geotechnical parameters, their effect on the overall structural response of the tunnel is limited for the Pardis Highway Tunnel. Nevertheless, incorporating these corrections improves the physical consistency of the calibrated parameters and therefore enhances the reliability of subsequent numerical analyses and design evaluations.

It should be emphasized that the analyses presented in Figure 12 were performed under conditions fully consistent with those adopted during the back analysis procedure. In other words, the preliminary back-calculated model was evaluated without introducing any stress relaxation corrections during the final tunnel response analysis.

From a practical design perspective, an important question is whether the final numerical analysis can instead be performed by applying the stress relaxation factor and stress relaxation rate corrections only during the final design stage while

retaining the geotechnical parameters obtained from an uncorrected back analysis. To investigate this issue, the results of this approach were compared with those obtained from the fully corrected procedure, in which the corrections were incorporated consistently during both the back analysis and the final design calculations (Figure 13).

The left column of Figure 13 presents the tunnel response obtained by applying the stress relaxation corrections only during the final design analysis. In contrast, the right column shows the fully corrected model (identical to the right-hand column of Figure 12). Compared with the fully corrected solution, the partially corrected model exhibits noticeably larger differences in the predicted ground displacements and plastic-zone distributions than those observed in Figure 12. Furthermore, the fully corrected model produces maximum axial forces and bending moments that are approximately 12% and 18% higher, respectively, than those obtained when the corrections are introduced only during the final design stage.

These differences are substantially larger than the approximately 3% variations observed when both the back analysis and the final design calculations are performed consistently. This finding indicates that applying stress relaxation corrections only during the final design stage underestimates the internal forces developed in the support system and may therefore lead to unconservative tunnel designs. Consequently, stress relaxation corrections should be incorporated consistently throughout both the back analysis and the subsequent design analyses to ensure physically representative geotechnical parameters, reliable structural predictions, and overall consistency in the numerical modelling procedure.

5. Discussion of Model Limitations and Uncertainty

The proposed integrated FDM–GA framework demonstrated robust and repeatable performance in the back analysis of the Pardis Highway Tunnel. The repeatability of the optimization procedure was evaluated through 30 independent genetic algorithm (GA) runs, each initiated from a different randomly generated population. Despite the stochastic nature of the optimization process, the calibrated geotechnical parameters converged to relatively narrow ranges and consistently produced low objective function values. These observations indicate that the proposed framework provides stable and reliable parameter estimations for the investigated case study. Nevertheless, several limitations and sources of uncertainty should be considered when interpreting the results and assessing the broader applicability of the proposed methodology.

First, the numerical analyses were performed using 2D plane strain models. Although this approach substantially reduces the computational cost and makes repeated optimization practical, it cannot fully reproduce the 3D stress redistribution and face effects that occur during tunnel excavation. In the present study, these 3D excavation effects were represented through the stress relaxation factor and stress relaxation rate derived from the LDP. While this approach is widely accepted in practical tunnel engineering, fully 3D back analysis procedures could provide a more rigorous representation of the excavation process and may further improve parameter calibration.

Second, the ground behaviour was represented using the Mohr–Coulomb constitutive model. Owing to its simplicity, computational efficiency, and limited number of input parameters, this model is widely used in engineering practice and is particularly suitable for automated optimization procedures. However, it cannot represent more complex rock mass behaviour, including strain softening, anisotropy, brittle failure, or time-dependent deformation. Extending the proposed framework to more advanced constitutive models, such as the Hoek–Brown criterion or strain softening formulations, represents an important direction for future research.

Third, the calibration procedure relied exclusively on tunnel convergence measurements obtained from the monitoring system. Although tunnel convergence provides valuable information regarding the global deformation response of the excavation, additional monitoring data, such as extensometer measurements, surface settlements, stress measurements, or lining loads, could provide complementary constraints for the optimization process. Integrating multiple sources of field data would further reduce the non-uniqueness of the calibrated parameter sets and improve the reliability of the estimated geotechnical properties.

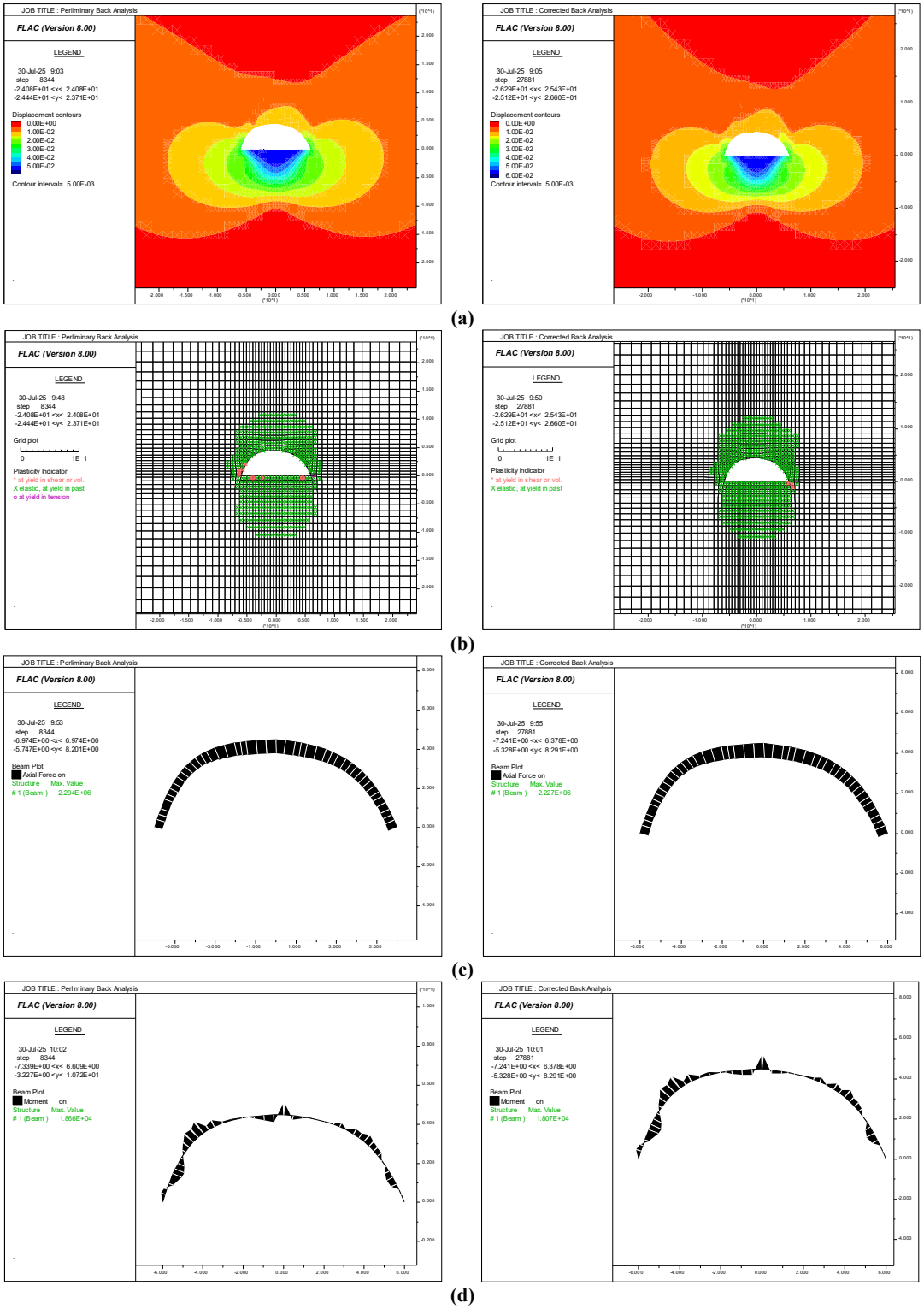

Figure 12. Comparison of (a) ground deformation patterns, (b) plastic zones, (c) support axial forces, and (d) support bending moments between the preliminary back-calculated model (left column) and the model corrected for stress relaxation factor and rate (right column)

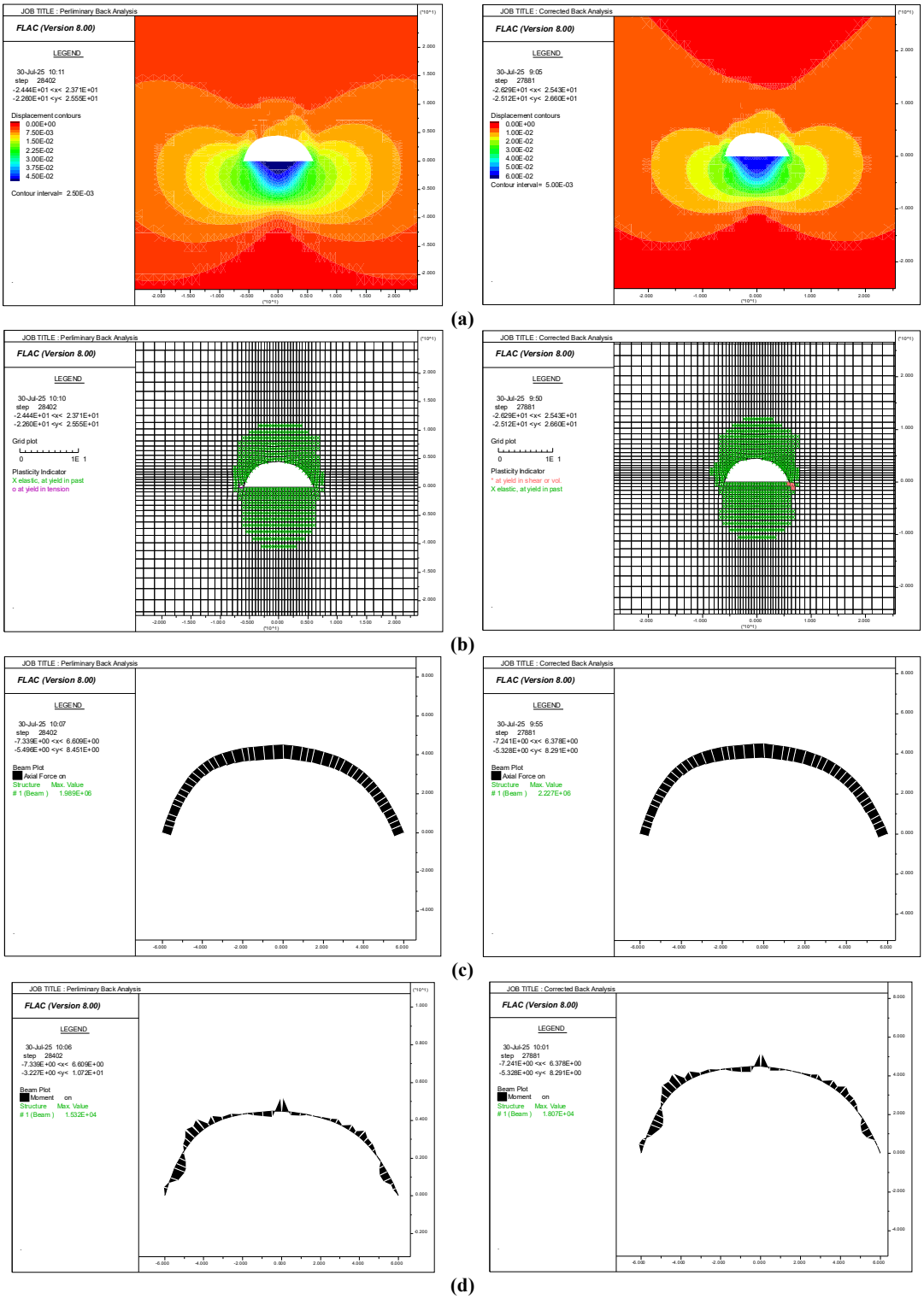

Figure 13. Comparison of tunnel response when stress relaxation factor and rate corrections are applied only at the final design stage (left column) versus when corrections are applied during both back-analysis and final calculations (right column) for (a) ground deformation patterns, (b) plastic zones, (c) support axial forces, and (d) support bending moments

In addition to these modelling assumptions, several sources of uncertainty remain inherent in the back analysis process. The measured tunnel convergences are subject to uncertainties associated with instrument precision, installation accuracy of convergence pins, field measurement procedures, and the natural spatial variability of the rock mass. Furthermore, the representative convergence values adopted in this study were obtained by fitting power-law relationships to measurements collected from multiple monitoring stations. Although this procedure reduces the influence of local variations and provides a consistent calibration dataset, some uncertainty associated with measurement scatter and the regression process inevitably remains.

Another important source of uncertainty arises from the inherent non-uniqueness of inverse analysis problems. Different combinations of geotechnical parameters may produce similar displacement responses and comparable objective function values, making it impossible to identify a unique solution based solely on numerical optimization. Rather than treating the optimized parameters as unique physical properties of the rock mass, they should therefore be interpreted as representative engineering parameters that best reproduce the observed field behaviour under the adopted modelling assumptions. To reduce this ambiguity, the present study combined the optimization results with independent geological evidence obtained from comparable tunnel projects. It also employed the observed inter-parameter correlations to identify the most representative engineering parameters. This integrated interpretation substantially reduced the range of acceptable parameter combinations and improved the engineering credibility of the final calibrated parameter set.

The sensitivity analyses presented in this study further demonstrated that both the initial stress relaxation factor and the stress relaxation rate have a measurable influence on the calibrated geotechnical parameters, although their effects differ. These findings highlight the importance of accurately representing 3D excavation effects in 2D tunnel back analysis procedures and demonstrate that stress relaxation should be regarded as a primary calibration variable rather than a secondary modelling assumption.

Future developments of the proposed framework may therefore focus on several complementary directions. In particular, future studies should investigate the applicability and performance of the integrated FDM–GA framework when coupled with fully 3D numerical models and more advanced constitutive laws, such as the Hoek–Brown criterion and strain softening models. Such developments would enable direct simulation of tunnel face effects without relying on equivalent stress relaxation parameters while providing a more realistic representation of complex rock mass behaviour. The integration of additional field monitoring data would further constrain the optimization process and reduce parameter non-uniqueness. Finally, probabilistic inverse analysis techniques, Bayesian parameter estimation, and uncertainty propagation methods may be incorporated to quantify confidence intervals for the calibrated parameters and explicitly account for measurement uncertainty during the optimization process. These developments would further enhance the robustness, reliability, and practical applicability of the integrated FDM–GA framework for tunnel back analysis.

5. Conclusions

- The integrated FDM–GA framework was successfully applied to the back analysis of the Pardis Highway Tunnel, enabling the calibration of the geotechnical properties of the Hezar Darreh conglomerate using representative tunnel convergence measurements.
- The observed correlations between cohesion and friction angle, as well as between Young's modulus and the coefficient of lateral earth pressure at rest, significantly reduced the non-uniqueness of the inverse analysis problem and facilitated the identification of a representative, geologically consistent set of geotechnical parameters.
- Comparison with independent geotechnical data from similar regional tunnel projects provided external validation of the calibrated parameters. It demonstrated the value of integrating optimization results with geological evidence when selecting representative engineering parameters.
- A secondary GA optimization performed with fixed values of E, c, φ, and K_0 produced consistent estimates of density (ρ) and Poisson's ratio (υ), further confirming the repeatability and robustness of the proposed framework. Nevertheless, the calibrated parameters should be interpreted as representative engineering properties rather than unique physical characteristics of the rock mass because of measurement uncertainty and the inherent non-uniqueness of inverse analysis problems.

- The results further demonstrated that stress relaxation corrections should be applied consistently throughout both the back analysis and the subsequent design analyses. Applying these corrections only during the final design stage led to underestimation of the internal forces developed in the tunnel support system, highlighting the importance of maintaining modelling consistency throughout the analysis process.
- Overall, Part II demonstrates that the integrated FDM–GA framework provides a robust, repeatable, and practical methodology for tunnel back analysis. By combining automated optimization, geological interpretation, inter-parameter correlation analysis, and systematic evaluation of stress relaxation effects, the proposed framework improves the reliability and engineering interpretation of calibrated geotechnical parameters. It also provides a solid basis for future developments involving the integration of multiple field monitoring data (e.g., extensometer measurements, stress measurements, lining loads, and surface settlements), advanced constitutive models, fully 3D numerical analyses, and probabilistic uncertainty quantification.

References

[1]. Moreira, N., Miranda, T., Pinheiro, M., Fernandes, P., Dias, D., Costa, L., & Sena-Cruz, J. (2013). Back analysis of geomechanical parameters in underground works using an Evolution Strategy algorithm. *Tunnelling and Underground Space Technology*, 33, 143-158.

[2]. Sun, J., Wang, F., Wang, X., & Wu, X. (2021). A Quantitative Evaluation Method Based on Back Analysis and the Double-Strength Reduction Optimization Method for Tunnel Stability. *Advances in Civil Engineering*, 2021(1), 8899685.

[3]. Chang, X., Wang, H., & Zhang, Y. (2023). Back analysis of rock mass parameters in tunnel engineering using machine learning techniques. *Computers and Geotechnics*, 163, 105738.

[4]. Zhang, C., Chen, Q., Zhou, W., & Huang, X. (2025). Inversion of mechanical parameters of tunnel surrounding rock based on improved gwo-bp neural network. *Applied Sciences*, 15(2), 537.

[5]. Pang, Z., Huang, Y., Xie, M., & Liu, Y. (2025). A physics-informed framework for mechanical parameters inversion in tunnel engineering based on deep learning and Bayesian optimization. *Tunnelling and Underground Space Technology*, 166, 106940.

[6]. Iran Oston Cons. Engs. (2022). The second phase geological and complementary studies report for Tunnel No. 1 (Northern Tehran Highway) project.

[7]. Payab Zamzam Cons. Engs. (2023). Instrumentation and convergencemetery reports for Tunnels No. 1 (Northern Tehran Highway) project.

[8]. Boggs, S. (2012). Principles of sedimentology and stratigraphy.

[9]. Bell, F. (1978). The physical and mechanical properties of the fell sandstones, Northumberland, England. *Engineering Geology*, 12, 1-29.

[10]. Howarth, D.F., & Rowlands, J.C. (1986). Development of an index to quantify rock texture for qualitative assessment of intact rock properties. *Geotechnical Testing Journal*, 9(4), 169-179.

[11]. Shakoor, A., & Bonelli, R.E. (1991). Relationship between petrographic characteristics, engineering index properties, and mechanical properties of selected sandstones. *Bulletin of the Association of Engineering Geologists*, 28(1), 55-71.

[12]. Shafiei, A. & Dusseault, M. (2008).Geomechanical properties of a conglomerate from Iran. in *ARMA US Rock Mechanics/Geomechanics Symposium*. Arma.

[13]. Jackson, R., Gorski, B., & Gyenge, M. (1995). Geotechnical properties of rock: A data base of physical properties of Canadian rock including both intact and residual strength, Canada Communication Group Publishing.

[14]. Bratton, J.L., & Pratt, H.R. (1968).Two-dimensional finite difference calculations of dynamic in-situ response of layered geologic media to a large explosive load. in *ARMA US Rock Mechanics/Geomechanics Symposium*. ARMA.

[15]. Boyum, B.H. (1961).Subsidence case histories in Michigan mines. in *ARMA US Rock Mechanics/Geomechanics Symposium*. ARMA.

[16]. Xiangjun, L., Jian, X., Lixi, L., & Xincai, Y. (2018). Rock mechanical characteristics and fracture propagation mechanism of sandy conglomerate reservoirs in Baikouquan formation of Mahu sag. *Xinjiang Petroleum Geology*, 39(zk (English)), 103.

[17]. Li, N., Zhang, S.C., Ma, X.F., Zou, Y.S., Chen, M., Li, S.H., & Zhang, Y.N. (2017). Experimental study on the propagation mechanism of hydraulic fracture in glutenite formations. *Chin. J. Rock Mech. Eng*, 36(10), 2383-2392.

[18]. Hoek, E. (2007). Practical rock engineering. 2007. *Online. ed. Rocscience*.

[19]. Goodman, R.E. (1991). Introduction to rock mechanics. John Wiley & Sons.

[20]. Majdi, A. (1998). Grouting design for Tehran Metro Tunnels (lines 1 and 2).

[21]. Moosavi, M. & Mohammadi Arimi, H. (2003). Stability analysis of Lavarak underground powerplant in Hezardarreh conglomerate formation based on

instrumentation data in *6th Iranian Tunneling Conference*.

[22]. Fakhimi, A., Salehi, D., & Mojtabai, N. (2004). Numerical back analysis for estimation of soil parameters in the Resalat Tunnel project. *Tunnelling and Underground Space Technology*, 19(1), 57-67.

[23]. Ebtekar, E., Sorush, A. & Yavari, M. (2001). Stability analysis of Resalat twin tunnels. in *1st Iranian Rock Mechanics Conference*.

[24]. Nouriyan Bidgoli, M. & Shahriyar, K. (2004). A method to determine the real ground geomechanical parameters using numerical methods. in *Iraniain Mining Conference*.

[25]. Potts, D.M., Zdravković, L., Addenbrooke, T., Higgins, K.G., & Kovačević, N. (2001). Finite element analysis in geotechnical engineering: application. Vol. 2. Thomas Telford London.

[26]. Boonyarak, T. & Ng, C.W. (2015). Effects of construction sequence and cover depth on crossing-tunnel interaction. *Canadian Geotechnical Journal*, 52(7), 851-867.

[27]. Lunardi, P. (2008). Design and construction of tunnels: Analysis of Controlled Deformations in Rock and Soils (ADECO-RS). Springer Science & Business Media.

[28]. Vlachopoulos, N., & Diederichs, M. (2009). Improved longitudinal displacement profiles for convergence confinement analysis of deep tunnels. *Rock mechanics and rock engineering*, 42, 131-146.

[29]. Panet, M. & Sulem, J. (2022). Convergence-confinement method for tunnel design. Springer.

[30]. Carranza-Torres, C. & Fairhurst, C. (2000). Application of the convergence-confinement method of tunnel design to rock masses that satisfy the Hoek-Brown failure criterion. *Tunnelling and underground space technology*, 15(2), 187-213.

انجمن مهندسی معدن ایران
نشریه مهندسی معدن و محیط زیست
نشانی نشریه: www.jme.shahroodut.ac.ir
دانشگاه صنعتی شاهرود

چارچوب یکپارچه FDM–GA برای تحلیل برگشتی خودکار در تونل‌سازی – بخش دوم: مطالعه موردی و تاثیر پارامترهای آزادسازی تنش

محمدتقی همزبان[1*]، علی‌رضا چهرقان[1]، و روزبه گرایلی میکلا[2]

۱- دانشیار دانشکده مهندسی معدن، دانشگاه صنعتی سهند، تبریز، ایران
۲- همکار ارشد، شرکت Delve Underground، والنات کریک، کالیفرنیا، ایالات متحده آمریکا

اطلاعات مقاله

تاریخ ارسال: ۲۰۲۵/۱۲/۰۶
تاریخ داوری: ۲۰۲۶/۰۷/۲۵
تاریخ پذیرش: ۲۰۲۶/۰۶/۳۱

DOI: 10.22044/jme.2026.17275.3422

کلمات کلیدی

تونل
مدل‌سازی عددی
تحلیل برگشتی
الگوریتم ژنتیک
آزادسازی تنش

چکیده

در مقاله بخش اول، یک چارچوب یکپارچه مبتنی بر روش تفاضل محدود–الگوریتم ژنتیک (FDM–GA) برای انجام خودکار تحلیل برگشتی تونل‌ها توسعه داده شد که در آن، شبیه‌سازی عددی با بهینه‌سازی تکاملی ترکیب گردید؛ تا پارامترهای ژئوتکنیکی، بر اساس داده‌های رفتارنگاری، برآورد شوند. در بخش دوم، کاربرد و اعتبارسنجی این چارچوب، با تحلیل برگشتی تونل بزرگراه پردیس، که در سازند کنگلومرایی هزاردره در شمال تهران حفاری شده است، بررسی می‌شود. داده‌های همگرایی سه‌نقطه‌ای ثبت‌شده در ۲۴ ایستگاه، پردازش شدند تا مقادیر مرجع جابجایی استخراج شوند. برای برآورد پارامترهای توده‌سنگ، ۳۰ اجرای مستقل از فرآیند بهینه‌سازی FDM–GA انجام شد که در نتیجه، بازه‌های کالیبره‌شده و محدودی برای چسبندگی (c)، زاویه اصطکاک داخلی (φ)، مدول یانگ (E) و ضریب فشار جانبی خاک در حالت سکون (K_0) به دست آمد. سپس، با تلفیق نتایج بهینه‌سازی، همبستگی میان پارامترها و شواهد ژئوتکنیکی حاصل از پروژه‌های تونل‌سازی مشابه، یک مقدار معرف برای پارامترهای یاد شده، تعیین شد. برخلاف مطالعات متداول تحلیل برگشتی تونل، که عمدتاً بر بهینه‌سازی پارامترها تمرکز دارند، چارچوب پیشنهادی علاوه بر فرآیند بهینه‌سازی، تفسیر زمین‌شناسی را نیز در نظر می‌گیرد؛ تا مجموعه‌ای از مقادیر معرف پارامترهای ورودی، شناسایی شود. همچنین، این چارچوب به‌صورت نظام‌مند، تاثیر فرضیات مربوط به آزادسازی تنش، بر کالیبراسیون پارامترها و تفسیر مهندسی نتایج کالیبره‌شده را ارزیابی می‌کند. محاسبه مجدد منحنی واکنش زمین (GRC) و پروفیل جابجایی طولی (LDP) نشان داد که حتی تغییرات نسبتاً کوچک در فرضیات مرتبط، تأثیر قابل‌توجهی بر میزان همگرایی پیش‌بینی‌شده و نیز پارامترهای ژئوتکنیکی کالیبره‌شده دارند. نتایج این پژوهش نشان داد که برآورد قابل‌اعتماد تغییرشکل‌های پیش از نصب سیستم نگهداری و میزان آزادشدگی تنش، شرطی اساسی برای انجام واقع‌بینانه تحلیل برگشتی تونل است. همچنین، این نتایج تأیید می‌کنند که چارچوب یکپارچه توسعه یافته FDM–GA ابزاری توانمند، پایدار و تکرارپذیر برای کالیبراسیون پارامترهای ژئوتکنیکی در پروژه‌های تونل‌سازی مبتنی بر روش نوین اتریشی (NATM) است.

نویسنده مسئول مکاتبات: hamzaban@sut.ac.ir (م. ت. همزبان)